THE JOURNAL OF PHYSICAL CHEMISTRY B

Article

Cite This: J. Phys. Chem. B 2019, 123, 239−246

pubs.acs.org/JPCB

Collective Mesoscale Dynamics of Liquid 1-Dodecanol Studied by Neutron Spin-Echo Spectroscopy with Isotopic Substitution and Molecular Dynamics Simulation

Tsuyoshi Yamaguchi,*[,†] Antonio Faraone,[‡] and Michihiro Nagao[‡,§]

[†]Graduate School of Engineering, Nagoya University, Furo-cho, Chikusa, Nagoya, Aichi 464-8603, Japan

[‡]NIST Center for Neutron Research, National Institute of Standards and Technology, Gaithersburg, Maryland 20899-6102, United States

[§]Center for Exploration of Energy and Matter, Indiana University, Bloomington, Indiana 47408-1398, United States

ABSTRACT: The collective dynamics of liquid 1-dodecanol was investigated at a length scale matching the mesoscale structure arising from the segregation of hydrophilic and hydrophobic domains. To this end, neutron spin-echo experiments were performed on a series of partially deuterated samples and the relevant collective dynamics of the hydroxyl groups with respect to the alkyl chains was extracted from the linear combination of the intermediate scattering functions of these samples. The resulting collective dynamics is slower than the single particle dynamics as determined by the measurement on the nondeuterated sample. The experimental results are in excellent agreement with molecular dynamics simulation, which allows further insight into the mechanism of the molecular motions. The results indicate that two factors are responsible for the slower collective dynamics. The first one is the slower dynamics of the hydroxyl group, with respect to the alkyl chains, owing to hydrogen bonding, and the second one is the presence of mesoscale structuring.

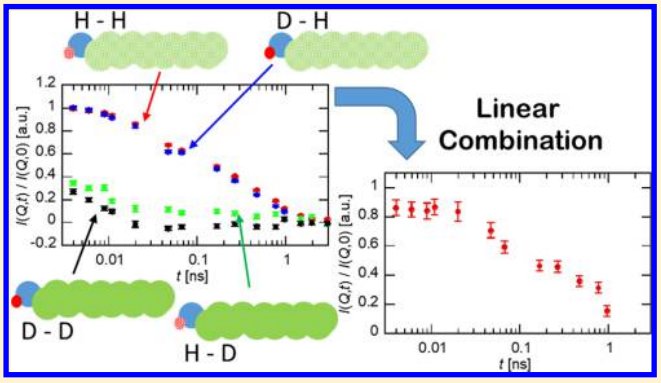

1. INTRODUCTION

1-Alcohols are one of the simplest amphiphilic molecules, in which a hydrophilic OH group is attached to the end of the hydrophobic alkyl chain. In their liquid state, OH groups aggregate through intermolecular hydrogen bonding, and alkyl chains excluded from the hydrogen bonding interaction also cluster together. As a result, liquid 1-alcohols exhibit a characteristic mesoscopic structure represented as "prepeak" in the static structure factor, which resembles the mesoscopic structure of surfactants. It is a question of fundamental relevance how this characteristic structuring of 1-alcohols affects their macroscopic properties.[1−3]

Viscoelastic spectra of liquid 1-alcohols are known to exhibit bimodal relaxation.[4−8] Our recent molecular dynamics (MD) simulation study demonstrated, from the comparison between the viscoelastic spectra and the intermediate scattering function (ISF), that the slower relaxation mode can be assigned to the coupling with the mesoscopic dynamics, whereas the faster mode can be ascribed to microscopic structural relaxation.[9] The picture obtained by the MD simulation was later confirmed experimentally on 3,7-dimethyl-1-octanol using γ-ray quasi-elastic scattering spectroscopy.[10] The crucial role of the mesoscale dynamics of 1-alcohols in determining their shear viscosity suggested by these studies seems natural considering that the mesoscopic structuring of surfactant systems is the origin of their large structural viscosity.[11]

The ISF of liquids is experimentally probed by quasielastic scattering spectroscopy of quantum beams such as X-ray or neutron. Provided that the viscoelastic relaxation of normal liquids occurs in the picoseconds to nanoseconds range, it is necessary to determine the ISF in this time region to probe the structural dynamics relevant to shear viscosity. Unfortunately, the prepeak signal is usually rather weak. Moreover, due to the large photon energy of X-ray, it is quite difficult for the X-ray quasielastic scattering to achieve the high energy resolution required. In the γ-ray quasielastic scattering study of 3,7-dimethyl-1-octanol, the dynamics in the 100 ns domain was determined using the narrow spectrum of the nuclear resonance of ^{57}Fe and time-domain interferometry, and it was necessary to extrapolate the viscoelastic relaxation time under ambient condition to supercooled temperatures.[10]

It is, in principle, more appropriate to use neutron for the determination of slow dynamics owing to the low energy of the incident beam. The combination of various neutron spectrometers can determine the liquid dynamics in a wide time window

Received: October 22, 2018
Revised: November 21, 2018
Published: December 4, 2018

DOI: 10.1021/acs.jpcb.8b10299
J. Phys. Chem. B 2019, 123, 239−246

ranging from femtoseconds to nanoseconds. We have successfully utilized neutron quasielastic spectroscopy to study various viscous liquids to resolve the microscopic origin of their shear viscosity.[12−17] Due to the large incoherent scattering cross section of protons, it is usual to use deuterated samples to measure the collective dynamics with neutron quasielastic scattering. Unfortunately enough, however, the static neutron structure factor of fully-deuterated 1-alcohols hardly exhibits the prepeak that represents the characteristic mesoscopic structure.[1,18] As a result, it is difficult to extract the collective dynamics of 1-alcohols associated with the prepeak structure from the neutron quasielastic scattering spectrum of fully-deuterated samples. However, isotopic substitution techniques offer a possible way to overcome this problem through the use of a combination of partially deuterated samples. Because the coherent scattering length of a deuteron is quite different from that of a proton, one can alter the scattering contrast of a desired group by means of selective deuteration. Such an experiment is routinely performed for structural determination using neutron diffraction with the support of computer simulation.[19] The local structure of a chosen group can then be extracted from the linear combination of diffraction patterns of partially deuterated samples.

We have demonstrated using *m*-toluidine,[20] glyceline,[21] and liquid methanol[22] that the linear combination analysis of partially deuterated samples is also possible for quasielastic neutron scattering spectra. In the work on methanol,[22] using linear combination of the ISFs of CH_3OH, CD_3OH, CH_3OD, and CD_3OD, the contribution of the incoherent scattering was eliminated, and the collective dynamics of the cross correlation between methyl and hydroxyl groups was extracted.

In this work, we apply the same analysis to 1-dodecanol, which is the longest 1-alcohol that shows liquid state under ambient condition. The ISFs at wavenumbers corresponding to the prepeak are determined for four samples, $C_{12}H_{25}OH$ (d_0), $C_{12}H_{25}OD$ (d_1), $C_{12}D_{25}OH$ (d_{25}), and $C_{12}D_{25}OD$ (d_{26}), by means of neutron spin-echo (NSE) spectroscopy, and the mesoscale collective dynamics is extracted from their linear combination. In addition, MD simulation is performed on the same system for comparison with the experiment and detailed analyses. In this way, we were able to experimentally determine the association between the mesoscale dynamics and the slower relaxation mode present in the dynamics of 1-dodecanol.

In the next section of the paper, the basic concepts and equations of NSE spectroscopy will be given, which, together with a brief overview of the common definitions of the dynamic structure factors, will allow for a detailed explanation of the isotopic substitution methodology employed to probe the mesoscopic dynamics of the prepeak. The following section will provide the information regarding the experimental and MD details. The experimental results, together with a comparison with the MD simulation, will be reported and discussed in Section 4, before the conclusion.

2. THEORETICAL BACKGROUND

In a neutron scattering experiment, a neutron beam is directed onto the sample and some of the neutrons, interacting with the nuclei of the sample, will exchange momentum and energy. For isotropic samples, the scattering pattern only depends on the moduli of the exchanged wave vector, $Q = |\boldsymbol{Q}| = |\boldsymbol{k}_f - \boldsymbol{k}_i|$, $\boldsymbol{k}_f$ and $\boldsymbol{k}_i$ being the final and initial wavevectors of the scattered neutron, respectively. For small values of energy exchanged between the scattered neutrons and the sample, Q is determined solely by the neutron wavelength and the scattering angle, θ: $Q = \frac{4\pi}{\lambda}\sin\left(\frac{\theta}{2}\right)$.

In a NSE experiment, a polarized neutron beam is employed, where the spins of all neutrons are aligned. The neutrons' spins are made to precess through two magnetic fields, created by solenoids aligned along the flight path, located before and after the sample. By scanning the difference between the magnetic field experienced by the neutrons, the field integral $J = \int B\, dl$ in the first and second arm, a typical echo signal is obtained, with the echo condition occurring when the field integrals in the first and second arm are the same. The amplitude of the measured echo, A^{echo}, is proportional to the energy Fourier transform of the double differential scattering cross section, $\frac{\partial^2\sigma}{\partial\Omega\partial E}$,[23] which represents the probability of a neutron to be scattered in the solid angle Ω, exchanging an energy E with the sample[24]

$$A^{\text{echo}}(Q, t) = \frac{1}{2} I_0^{\text{n}} VT \int_{-\infty}^{\infty} \left(\frac{\partial^2\sigma}{\partial\Omega\partial E}\right)^{\text{NSE}} \cos\left(\frac{Et}{\hbar}\right) dE\, d\Omega = \frac{1}{2} I_0^{\text{n}} VT I^{\text{NSE}}(Q, t) d\Omega \tag{1}$$

where I_0^{n} is the number of incoming neutrons, V is the sample volume in the beam, and the transmission, T, takes into account self-shielding effects.

Because of the dependence of each atom's neutron scattering cross section on their isotopic composition and, more importantly here, nuclear spin state, the neutron scattering signal can be considered as the sum of a coherent and incoherent component: $\frac{\partial^2\sigma}{\partial\Omega\partial E} = \left(\frac{\partial^2\sigma}{\partial\Omega\partial E}\right)_{\text{coh}} + \left(\frac{\partial^2\sigma}{\partial\Omega\partial E}\right)_{\text{inc}}$. The coherent scattering does not alter the neutron spin and the nuclear spin incoherent scattering has a 2/3 probability of flipping the neutron spin, so the double differential scattering cross section probed by NSE is given by

$$\left(\frac{\partial^2\sigma}{\partial\Omega\partial E}\right)^{\text{NSE}} = \left(\frac{\partial^2\sigma}{\partial\Omega\partial E}\right)_{\text{coh}} - \frac{1}{3}\left(\frac{\partial^2\sigma}{\partial\Omega\partial E}\right)_{\text{inc}} \tag{2}$$

During the NSE experiment, a polarized diffraction measurement is carried out for each experimental configuration. Two measurements are performed to obtain

$$I^{\text{UP}}(Q) = I_0^{\text{n}} VT\left[\left(\frac{\partial\sigma}{\partial\Omega}\right)_{\text{coh}} + \frac{1}{3}\left(\frac{\partial\sigma}{\partial\Omega}\right)_{\text{inc}}\right] d\Omega \tag{3}$$

$$I^{\text{DWN}}(Q) = I_0^{\text{n}} VT\frac{2}{3}\left(\frac{\partial\sigma}{\partial\Omega}\right)_{\text{inc}} d\Omega \tag{4}$$

So that

$$I^{\text{UP}}(Q) - I^{\text{DWN}}(Q) = I_0^{\text{n}} VT\left[\left(\frac{\partial\sigma}{\partial\Omega}\right)_{\text{coh}} - \frac{1}{3}\left(\frac{\partial\sigma}{\partial\Omega}\right)_{\text{inc}}\right] d\Omega = I_0^{\text{n}} VT\left(\frac{\partial\sigma}{\partial\Omega}\right)^{\text{NSE}} d\Omega \tag{5}$$

and

$$I^{\text{UP}}(Q) + I^{\text{DWN}}(Q) = I_0^{\text{n}} VT\frac{\partial\sigma}{\partial\Omega} d\Omega \tag{6}$$

DOI: 10.1021/acs.jpcb.8b10299
J. Phys. Chem. B 2019, 123, 239−246

where $\frac{\partial\sigma}{\partial\Omega} = \left(\frac{\partial\sigma}{\partial\Omega}\right)_{coh} + \left(\frac{\partial\sigma}{\partial\Omega}\right)_{inc}$ is the differential neutron scattering cross section, which represents the probability of a neutron to be scattered in the solid angle Ω subtended by the detector; $\left(\frac{\partial\sigma}{\partial\Omega}\right)_{coh}$ and $\left(\frac{\partial\sigma}{\partial\Omega}\right)_{inc}$ are its coherent and incoherent components, respectively; and the differential scattering cross section probed by NSE is given by $\left(\frac{\partial\sigma}{\partial\Omega}\right)^{NSE} = \left(\frac{\partial\sigma}{\partial\Omega}\right)_{coh} - \frac{1}{3}\left(\frac{\partial\sigma}{\partial\Omega}\right)_{inc}$.

For the polarized diffraction measurements, only $I^{UP}(Q)$ and $I^{DWN}(Q)$ are measured, which can be used to determine separately the coherent and incoherent differential scattering cross sections of the sample using standard formulas accounting for instrumental effects.[25]

The coherent and incoherent double differential scattering cross sections are directly related to the collective and single particle dynamic structure factors of the sample

$$\left(\frac{\partial^2\sigma}{\partial\Omega\partial E}\right)_{coh} = \frac{1}{N}\frac{k_f}{k_i}\sum_{\alpha=1}^{n}\sum_{\beta=1}^{n} b_\alpha^{coh} b_\beta^{coh}\sqrt{N_\alpha N_\beta}\, S_{coll}^{\alpha\beta}(Q, E) \tag{7}$$

$$\left(\frac{\partial^2\sigma}{\partial\Omega\partial E}\right)_{inc} = \frac{1}{N}\frac{k_f}{k_i}\sum_{\alpha=1}^{n} (b_\alpha^{inc})^2 S_s^{\alpha}(Q, E) \tag{8}$$

where n represents the number of different groups of atoms (e.g., H, C, O, ...) present in the sample; b_α^{coh} and b_α^{inc} are the coherent and incoherent scattering length of the isotope α in the sample, respectively; and N and N_α represent the total number of nuclei and nuclei of the isotope α in the sample, respectively.

The partial dynamic structure factors, $S_{coll}^{\alpha\beta}(Q,E)$, and the single particle dynamics structure factors, $S_s^{\alpha}(Q,E)$, are defined as

$$S_{coll}^{\alpha\beta}(Q, E) = \frac{1}{2\pi}\int_{-\infty}^{\infty} I_{coll}^{\alpha\beta}(Q, t)\exp(-iEt/\hbar)dt \tag{9}$$

$$I_{coll}^{\alpha\beta}(Q, t) = \frac{1}{\sqrt{N_\alpha N_\beta}}\sum_{i_\alpha=1}^{N_\alpha}\sum_{i_\beta=1}^{N_\beta}\langle\exp\{i\boldsymbol{Q}\cdot\boldsymbol{R}_{i_\alpha}(t)\}\exp\{i\boldsymbol{Q}\cdot\boldsymbol{R}_{i_\beta}(0)\}\rangle \tag{10}$$

$$S_s^{\alpha}(Q, E) = \frac{1}{2\pi}\int_{-\infty}^{\infty} I_s^{\alpha}(Q, t)\exp(-iEt/\hbar)dt \tag{11}$$

$$I_s^{\alpha}(Q, t) = \frac{1}{N_\alpha}\sum_{i_\alpha=1}^{N_\alpha}\langle\exp\{i\boldsymbol{Q}\cdot\boldsymbol{R}_{i_\alpha}(t)\}\exp\{i\boldsymbol{Q}\cdot\boldsymbol{R}_{i_\alpha}(0)\}\rangle \tag{12}$$

where $\boldsymbol{R}_{i_\alpha}(t)$ is the position of atom i_α at time t. The following notations are commonly employed:

$$S_y^x(Q) = \int_{-\infty}^{\infty} S_y^x(Q, E)dE = I_y^x(Q, t=0) = I_y^x(Q)$$

The neutron coherent, $I_{coh}^n(Q,t)$, and incoherent, $I_{inc}^n(Q,t)$, ISFs can be defined as

$$I_{coh}^n(Q, t) = \frac{1}{N}\frac{k_f}{k_i}\sum_{\alpha=1}^{n}\sum_{\beta=1}^{n} b_\alpha^{coh} b_\beta^{coh}\sqrt{N_\alpha N_\beta}\, I_{coll}^{\alpha\beta}(Q, t) \tag{13}$$

$$I_{inc}^n(Q, t) = \frac{1}{N}\frac{k_f}{k_i}\sum_{\alpha=1}^{n} (b_\alpha^{inc})^2 I_s^{\alpha}(Q, t) \tag{14}$$

$I^{NSE}(Q,t)$ of eq 1 is thus equal to

$$I^{NSE}(Q, t) = I_{coh}^n(Q, t) - \frac{1}{3}I_{inc}^n(Q, t) \tag{15}$$

NSE results are usually provided in terms of the normalized ISF

$$\frac{2A^{echo}(Q, t)}{I^{UP}(Q) - I^{DWN}(Q)} = \frac{I^{NSE}(Q, t)}{\left(\frac{\partial\sigma}{\partial\Omega}\right)^{NSE}} = \frac{I^{NSE}(Q, t)}{\int_{-\infty}^{\infty}\left(\frac{\partial^2\sigma}{\partial\Omega\partial E}\right)^{NSE}dE}$$
$$= \frac{I^{NSE}(Q, t)}{I^{NSE}(Q)} = \frac{I_{coh}^n(Q, t) - \frac{1}{3}I_{inc}^n(Q, t)}{I_{coh}^n(Q) - \frac{1}{3}I_{inc}^n(Q)} \tag{16}$$

so that instrumental effects, such as flipper efficiency, detector efficiency, incoming beam polarization, and so forth, cancel out. The finite instrumental resolution is taken into account by normalizing the data using the results obtained for a purely elastic sample measured under the same experimental condition.

1-Dodecanol is formed by the following groups of atoms: C, HC (the 25 hydrogens of the alkyl chain), HH (the hydrogen of the hydroxyl group), and O. Therefore, 4 single particle partial dynamics structure factors, S_s^C, S_s^{HC}, S_s^{HH}, and S_s^O, and the following 10 partial dynamic structure factors can be defined: S^{CC}, S^{CHC}, S^{CHH}, S^{CO}, S^{HCHC}, S^{HCHH}, S^{HCO}, S^{HHHH}, S^{HHO}, and S^{OO}. These partial dynamic structure factors are independent of the isotopic composition of the samples within the assumption of negligible isotopic effect. Although the difference in the hydrogen-bonding strengths of O−H and O−D groups may affect the dynamics of dodecanol, we consider its effect to be marginal because the same procedure worked well on liquid methanol.[22] Their double differential cross sections are then given by

$$\left(\frac{\partial^2\sigma}{\partial\Omega\partial E}\right)_{coh}^{d_x} = \frac{1}{N}\sum_{\alpha=1}^{4}\sum_{\beta=1}^{4} b_{\alpha_{d_x}}^{coh} b_{\beta_{d_x}}^{coh}\sqrt{N_\alpha N_\beta}\, S_{coll}^{\alpha\beta}(Q, E) \tag{17}$$

$$\left(\frac{\partial^2\sigma}{\partial\Omega\partial E}\right)_{inc}^{d_x} = \frac{1}{N}\sum_{\alpha=1}^{4} (b_{\alpha_{d_x}}^{inc})^2 S_s^{\alpha}(Q, E) \tag{18}$$

where x can be 26, 25, 1, or 0.

The following quantities can be defined

$$\left(\frac{\partial^2\sigma}{\partial\Omega\partial E}\right)_{coh}^{d_{25}} + \left(\frac{\partial^2\sigma}{\partial\Omega\partial E}\right)_{coh}^{d_1} - \left[\left(\frac{\partial^2\sigma}{\partial\Omega\partial E}\right)_{coh}^{d_{26}} + \left(\frac{\partial^2\sigma}{\partial\Omega\partial E}\right)_{coh}^{d_0}\right]$$
$$= \frac{1}{N}\sum_{\alpha=1}^{4}\sum_{\beta=1}^{4}\left[b_{\alpha_{d_{25}}}^{coh} b_{\beta_{d_{25}}}^{coh} + b_{\alpha_{d_1}}^{coh} b_{\beta_{d_1}}^{coh} - \left(b_{\alpha_{d_{26}}}^{coh} b_{\beta_{d_{26}}}^{coh} + b_{\alpha_{d_0}}^{coh} b_{\beta_{d_0}}^{coh}\right)\right]\sqrt{N_\alpha N_\beta}\, S_{coll}^{\alpha\beta}(Q, E)$$
$$= \frac{2\sqrt{25}}{N}\left[2b_D^{coh} b_H^{coh} - \left(b_D^{coh}\right)^2 - \left(b_H^{coh}\right)^2\right] S_{coll}^{HCHH}(Q, E) = -\frac{2\sqrt{25}}{N}\left(b_D^{coh} - b_H^{coh}\right)^2 S_{coll}^{HCHH}(Q, E) \tag{19}$$

$$\left(\frac{\partial^2\sigma}{\partial\Omega\partial E}\right)_{inc}^{d_{25}} + \left(\frac{\partial^2\sigma}{\partial\Omega\partial E}\right)_{inc}^{d_1} - \left[\left(\frac{\partial^2\sigma}{\partial\Omega\partial E}\right)_{inc}^{d_{26}} + \left(\frac{\partial^2\sigma}{\partial\Omega\partial E}\right)_{inc}^{d_0}\right]$$
$$= \frac{1}{N}\sum_{\alpha=1}^{4}\left[(b_{\alpha_{d_{25}}}^{inc})^2 + (b_{\alpha_{d_1}}^{inc})^2 - (b_{\alpha_{d_{26}}}^{inc})^2 - (b_{\alpha_{d_0}}^{inc})^2\right] S_s^{\alpha}(Q, E) = 0 \tag{20}$$

Therefore

DOI: 10.1021/acs.jpcb.8b10299
J. Phys. Chem. B 2019, 123, 239−246

$$\left(\frac{\partial^2\sigma}{\partial\Omega\partial E}\right)_{\text{combo}} = \left(\frac{\partial^2\sigma}{\partial\Omega\partial E}\right)^{d_{25}} + \left(\frac{\partial^2\sigma}{\partial\Omega\partial E}\right)^{d_1} - \left(\frac{\partial^2\sigma}{\partial\Omega\partial E}\right)^{d_{26}} - \left(\frac{\partial^2\sigma}{\partial\Omega\partial E}\right)^{d_0}$$
$$= -\frac{2\sqrt{25}}{N}(b_D^{coh} - b_H^{coh})^2 S_{coll}^{HCHH}(Q, E) \quad (21)$$

To take advantage of these identities, the data have to be properly normalized for the neutron flux, transmittance, and sample volume. In the case of polarized diffraction, this leads to the following equations

$$I_{combo}(Q) = I_{combo}^{coh}(Q)$$
$$= \frac{I_{d_{25}}^{coh}(Q)}{I_{d_{25}}^{monitor} V_{d_{25}} T_{d_{25}}} + \frac{I_{d_1}^{coh}(Q)}{I_{d_1}^{monitor} V_{d_1} T_{d_1}} - \frac{I_{d_{26}}^{coh}(Q)}{I_{d_{26}}^{monitor} V_{d_{26}} T_{d_{26}}} - \frac{I_{d_0}^{coh}(Q)}{I_{d_0}^{monitor} V_{d_0} T_{d_0}} \propto -S_{coll}^{HCHH}(Q) , \quad (22)$$

$$I_{combo}^{inc}(Q) = \frac{I_{d_{25}}^{inc}(Q)}{I_{d_{25}}^{monitor} V_{d_{25}} T_{d_{25}}} + \frac{I_{d_1}^{inc}(Q)}{I_{d_1}^{monitor} V_{d_1} T_{d_1}} - \frac{I_{d_{26}}^{inc}(Q)}{I_{d_{26}}^{monitor} V_{d_{26}} T_{d_{26}}} - \frac{I_{d_0}^{inc}(Q)}{I_{d_0}^{monitor} V_{d_0} T_{d_0}} = 0 , \quad (23)$$

where the monitor count, $I_{d_x}^{\text{monitor}}$, is proportional to the total neutron flux on the sample.

Analogously, for the NSE data

$$\frac{I_{combo}(Q,t)}{I_{combo}(Q)} = \frac{\frac{2A_{d_{25}}^{echo}(Q,t)}{I_{d_{25}}^{monitor} V_{d_{25}} T_{d_{25}}} + \frac{2A_{d_1}^{echo}(Q,t)}{I_{d_1}^{monitor} V_{d_1} T_{d_1}} - \frac{2A_{d_{26}}^{echo}(Q,t)}{I_{d_{26}}^{monitor} V_{d_{26}} T_{d_{26}}} - \frac{2A_{d_0}^{echo}(Q,t)}{I_{d_0}^{monitor} V_{d_0} T_{d_0}}}{\frac{|I_{d_{25}}^{UP}(Q) - I_{d_{25}}^{DWN}(Q)|}{I_{d_{25}}^{monitor} V_{d_{25}} T_{d_{25}}} + \frac{|I_{d_1}^{UP}(Q) - I_{d_1}^{DWN}(Q)|}{I_{d_1}^{monitor} V_{d_1} T_{d_1}} - \frac{|I_{d_{26}}^{UP}(Q) - I_{d_{26}}^{DWN}(Q)|}{I_{d_{26}}^{monitor} V_{d_{26}} T_{d_{26}}} - \frac{|I_{d_0}^{UP}(Q) - I_{d_0}^{DWN}(Q)|}{I_{d_0}^{monitor} V_{d_0} T_{d_0}}} = \frac{I_{coll}^{HCHH}(Q,t)}{I_{coll}^{HCHH}(Q)} , \quad (24)$$

3. EXPERIMENTAL SECTION[A]

3.1. Samples. The d_{26}, d_{25}, and d_1 samples were purchased from CDN isotopes and have 98% nominal deuteration. The d_0, protonated sample, was purchased from Sigma-Aldrich. All samples were employed without further purification.

3.2. Neutron Spectroscopy. Neutron scattering measurements were performed using the NSE spectrometer at the National Institute of Standards and Technology (NIST) Center for Neutron Research (NCNR). Measurements were performed using an average incoming wavelength, λ, of 5 Å with a $\Delta\lambda/\lambda$ of ≈17%.

For the polarized diffraction measurements, the samples were contained in standard flat titanium cells with a neutron path length of 1 mm, for the d_{26} and d_{25} samples, and 0.25 mm, for the d_1 and d_0 samples. During the experiment, the samples were maintained at 35 ± 0.5 °C using a thermal bath. For the NSE measurements, the samples were shaped as thin annuluses and contained in aluminum cans. The radial thickness of the samples was 0.2 mm, for the d_{26} and d_{25} samples, and 0.1 mm, for the d_1 and d_0 samples. Such thicknesses were chosen to maintain the multiple scattering contributions within acceptable limits; in fact, for all samples, the transmission was measured to be above 80%. The temperature of the samples was 28 ± 0.5 °C, controlled using a closed cycle refrigerator.

Transmission was measured for each sample and normalized to the direct beam. For the polarized diffraction measurements, the sample volume was estimated by assuming 98% deuteration and imposing agreement between the theoretical and experimental ratios of the incoherent intensity at $Q \to 0$ for the different samples. For the NSE measurements, several methods to estimate the sample volume were employed, all of the results coinciding with those obtained simply using the nominal thickness of the samples.

3.3. Molecular Dynamics Simulation. The MD simulation of liquid 1-dodecanol-d_0 was performed under *NVT* ensemble using the GROMACS 5.1.2 package.[26] The details of the simulation conditions were described in the literature.[9] The temperature of the system was 298 K, and the density was fixed to the experimental value at 298 K and 1 bar.[27] The TraPPE-UA model was employed to describe intra- and intermolecular interactions of 1-dodecanol.[28,29] In the TraPPE-UA model, the CH_3 and CH_2 groups were treated as united atoms. The length of the equilibration run was 100 ns, and three production runs of 1 μs length were performed. The correlation functions obtained from the three production runs were averaged.

Calculations of the static structure factor and ISF were performed directly in the reciprocal space. The coherent scattering lengths and the incoherent scattering cross sections of the united atoms were calculated as the sums of the respective values of constituent atoms. The correlation functions of the deuterated samples were calculated from the MD run of 1-dodecanol-d_0 under the assumption that the effects of deuteration on the static structure and the dynamics of the system are negligible. The weighted sums of the values of proton and deuteron were used for the coherent scattering length and the incoherent scattering cross section of the hydrogen of 98% deuterated samples.

4. RESULTS AND DISCUSSION

4.1. Diffraction. The diffraction patterns determined with the NSE spectrometer are reported in Figure 1. The intensities

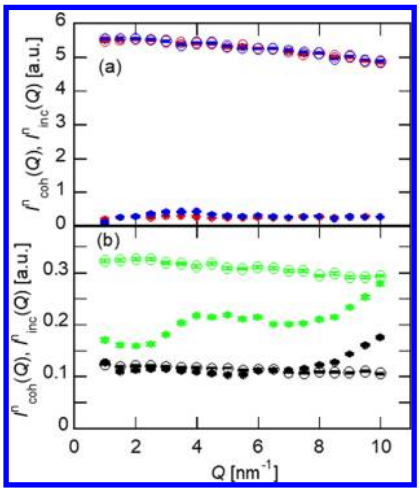

Figure 1. Coherent and incoherent neutron diffraction patterns of the four samples investigated are shown. The diffraction patterns of the d_0 (red) and d_1 (blue) samples are shown in panel (a), whereas those of d_{25} (green) and d_{26} (black) are in panel (b). The coherent and incoherent contributions are plotted with filled and open symbols, respectively. Error bars represent ±1 standard deviation throughout the paper.

of these diffractions were normalized with respect to the transmittance and the volume of the samples. The strength of the incoherent scattering decreases with deuteration as expected. The incoherent scattering overwhelms the coherent one in the cases of d_0 and d_1, whereas the coherent and the incoherent parts are comparable to each other in d_{25} and d_{26}.

The coherent diffraction patterns of the four samples are compared in Figure 2a. The prepeak is hardly observed in the fully deuterated sample, d_{26}, whereas the other three samples exhibit broad prepeaks at around 4 nm^{-1}. Closely compared, the position of the prepeak of d_{25} is a little higher than those of d_0 and d_1.

DOI: 10.1021/acs.jpcb.8b10299
J. Phys. Chem. B 2019, 123, 239−246

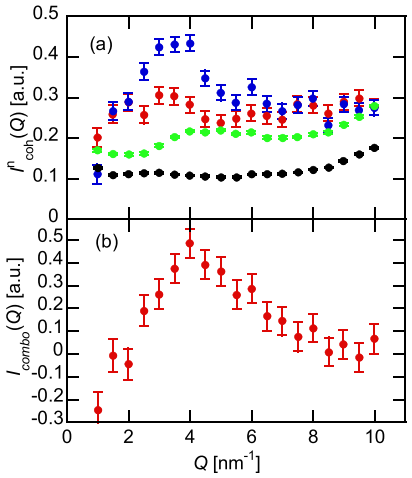

Figure 2. Coherent neutron diffraction patterns of the d_0 (red), d_1 (blue), d_{25} (green), and d_{26} (black) samples are shown in panel (a), and their combination, $I_{combo}(Q)$ defined by eq 22, is plotted in panel (b).

Figure 2b shows $I_{combo}(Q)$, experimentally determined from the diffraction patterns of the four samples, which describes, as shown in eq 22, the negative of the cross correlation between the hydrogen atoms of the alkyl and hydroxyl groups. The prepeak is clearly observed at 4 nm^{-1}, indicating that the prepeak is the signature of the mesoscopic structure composed of alkyl and hydroxyl domains.

Figure 3a shows the neutron diffraction patterns calculated by MD simulation. The simulation result is in good agreement with

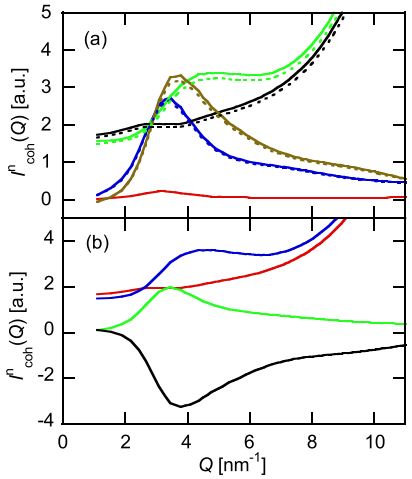

Figure 3. Neutron static structure factors calculated by MD simulation are plotted in panel (a). The structure factors of the d_0 (red), d_1 (blue), d_{25} (green), and d_{26} (black) samples are shown together with $I_{combo}(Q)$ (beige). The results of 100% d and 98% d cases are drawn with solid and dotted curves, respectively, to show the effects of incomplete deuteration. The value of 98% d was taken from the nominal value provided by the supplier of the deuterated reagents. In panel (b), the structure factor of d_{26} sample (red) is divided into the alkyl(HC + C)−alkyl (blue), hydroxyl(HH + O)−hydroxyl (green), and alkyl−hydroxy (black) correlations.

the experiment. Diffraction of the partially deuterated samples, d_1 and d_{25}, shows strong prepeaks, whereas that of the fully deuterated one, d_{26}, scarcely exhibits the prepeak. The difference in the peak positions of d_1 and d_{25} is also reproduced by the MD simulation. Combination analysis was also performed on the MD simulation data. A strong peak is observed in $I_{combo}(Q)$ at 4 nm^{-1}, which is also in harmony with the experiment.

In Figure 3b, the structure factor of d_{26} is divided into the contributions of the alkyl−alkyl, hydroxyl−hydroxyl, and alkyl−hydroxyl correlations, where alkyl and hydroxyl refer to the contributions of HC + C and HH + O, respectively. Both the calculations on the 98% d and 100% d case are plotted, the results being essentially the same. The autocorrelations of both the alkyl and the hydroxyl groups clearly exhibit the prepeaks, and the cross correlation shows a strong anticorrelation peak, which is consistent with the positive peak of $I_{combo}(Q)$. The absence of the prepeak in the neutron static structure factor of d_{26} is thus ascribed to the cancellation of these peaks, which in turn can be explained as a lack of scattering contrast between the hydroxyl and alkyl regions.

The position of the prepeak of the alkyl−alkyl correlation in Figure 3b is a little higher than that of the hydroxyl−hydroxyl correlation. The former is close to the peak position of the d_{25} prepeak, whereas the latter is closer to that of the d_1 prepeak. Therefore, the contribution of the alkyl group is stronger in the d_{25} diffraction, whereas that of the hydroxyl group is stronger in the d_1 diffraction, which explains the difference in the positions of their prepeaks.

In summary, the experimental data validate the results of the MD simulation. These, in turn, put in evidence the existence of two characteristic lengths at the mesoscale, the distances between the alkyl and hydroxyl groups, respectively. The signal of $I_{combo}(Q)$ instead arises from the alkyl−hydroxyl correlation and is located in between these two length scales, closer to the characteristic distance between the alkyl chains.

4.2. Dynamics. Figure 4 shows the ISFs of the four samples determined with NSE spectroscopy. The decays of $I^{NSE}(Q,t)/$

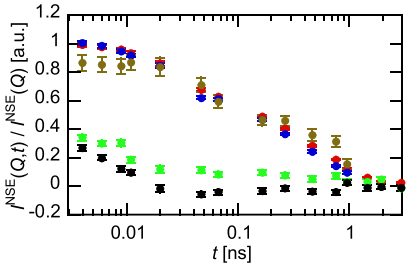

Figure 4. NSE normalized ISFs, $I^{NSE}(Q,t)/I^{NSE}(Q)$, of d_0 (red), d_1 (blue), d_{25} (green), and d_{26} (black) at $Q = 4$ nm^{-1} are plotted together with the combination results (beige), $I_{combo}(Q,t)$, as defined by eq 24.

$I^{NSE}(Q)$ of d_0 and d_1 are monomodal, whereas those of d_{25} and d_{26} are more complicated. The NSE ISF is determined, as shown by eq 15, by both coherent and incoherent scatterings. Considering the large number of protons in d_0 and d_1, it can be easily inferred that the incoherent part dominates the ISFs of these samples. In the cases of d_{25} and d_{26}, however, it cannot be said a priori which part is dominant, and the complicated time profile suggests the superposition of these two contributions.

The NSE ISFs are calculated from MD simulation, and the results are plotted in Figure 5. The calculations of both the 100% d and the 98% d cases were performed. In contrast to the static structure factor, the incomplete degree of the deuteration strongly affects the time profiles of the NSE ISFs of d_{25} and d_{26}. Given the large number of hydrogen atoms in the dodecyl group and the large incoherent scattering cross section of protons,

DOI: 10.1021/acs.jpcb.8b10299
J. Phys. Chem. B 2019, 123, 239−246

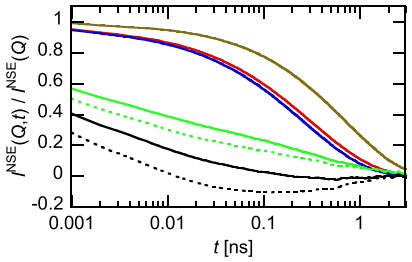

Figure 5. NSE ISFs of d_0 (red), d_1 (blue), d_{25} (green), and d_{26} (black) samples at $Q = 4.09$ nm^{-1} are calculated by MD simulation and plotted together with the combination results (beige), $I_{combo}(Q,t)$, as defined by eq 24. The solid and dotted curves show the 100% d and 98% d cases, respectively. These two curves overlap with each other in the cases of d_1 and $I_{combo}(Q,t)$.

small contamination of protons leads to the significant increase in the contribution of the incoherent component.

Comparing the experiment and simulation, the former agrees well with the 98% d case of the latter. In particular, the slightly negative value of $I^{NSE}(Q,t)/I^{NSE}(Q)$ of d_{26} at 0.02 ns < t < 1 ns is reproduced by the simulation. Therefore, we conclude that it is necessary to include the incomplete degree of deuteration to analyze the NSE signals of d_{25} and d_{26}, and our MD simulation works well to describe the NSE ISFs.

The total NSE ISFs are divided into their coherent and incoherent parts in Figure 6. The ISF of d_0 is almost exclusively determined by the incoherent part, as expected. The coherent part is not negligible in the d_1 case, but the incoherent part is still dominant. The situation is quite different in the d_{25} and d_{26} cases. The amplitudes of the coherent and the incoherent contributions are close to each other, and their relaxation rates are also comparable in the 100 ps domain. As a result, these two contributions cancel each other, and the amplitudes of $I^{NSE}(Q,t)/I^{NSE}(Q)$ for d_{25} and d_{26} become small in the 100 ps range.

As already explained in Section 2, the linear combination of the NSE data of these four samples, according to eq 24, eliminates the incoherent contributions and allows the extraction of the collective dynamics. This analysis is performed on both experiment and MD simulation, and their results are shown in Figures 4 and 5, respectively. The experimental result of $I_{combo}(Q,t)$ agrees qualitatively well with that from the MD simulation, which supports the validity of the combination analysis. In particular, although the contribution of the coherent component is minor in all four samples, the combination analysis can extract the coherent dynamics buried in these signals. Moreover, a specific partial ISF, such as $I^{HCHH}(Q,t)$, is not usually directly accessible experimentally; in particular, this one, yielding information on the dynamics of the hydroxyl groups with respect to the alkyl chains, has been shown in methanol to provide specific information on the time scale of hydrogen bonding in mesoscale associates.[22]

The relaxation of the collective dynamics, $I_{combo}(Q,t)/I_{combo}(Q)$, is compared with that of the single particle dynamics, $\frac{I_{d_0}^{NSE}(Q,t)}{I_{d_0}^{NSE}(Q)} \approx \frac{I_{d_0}^{inc}(Q,t)}{I_{d_0}^{inc}(Q)}$, for d_0 in Figure 7. The former appears slightly slower than the latter in both experiment and MD simulation. To extract their mean relaxation time, we fitted the relaxation of the ISFs with the Kohlrausch–Williams–Watts (KWW) function as

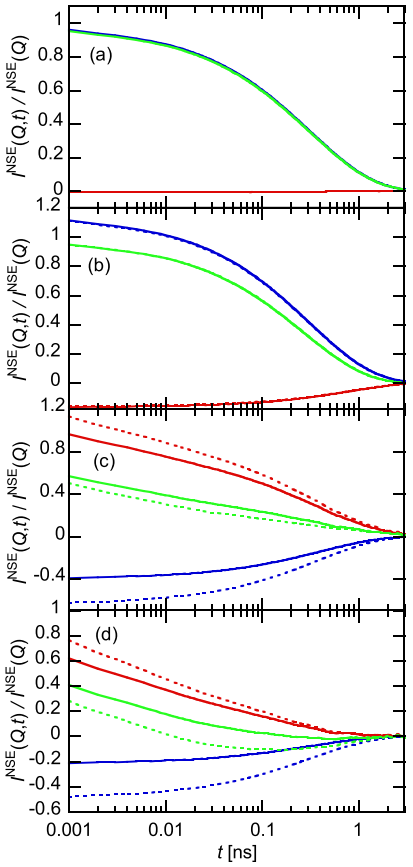

Figure 6. Total NSE ISFs (green) of the (a) d_0, (b) d_1, (c) d_{25}, and (d) d_{26} samples calculated by MD simulation are divided into coherent (red) and incoherent (blue) parts. The solid and dotted curves show the results of the 100% d and 98% d cases, respectively. These functions are normalized to the initial values of their respective total NSE ISFs.

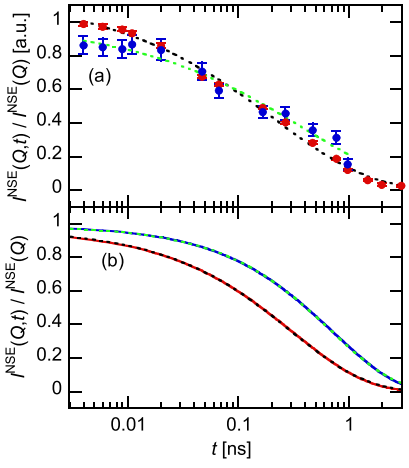

Figure 7. ISF of d_0 (red) is compared with $I_{combo}(Q,t)$ (blue). The results of the NSE experiment and MD simulation are shown in panels (a,b), respectively. These functions are normalized to their respective initial values. The black and green dotted curves exhibit the KWW fitting functions of $I_{d_0}^{NSE}(Q, t)$ and $I_{combo}(Q,t)$, respectively.

$$I^{KWW}(t) = A \exp\left[-\left(\frac{t}{\tau}\right)^{\beta}\right] \tag{25}$$

The mean relaxation time of the KWW function, $\langle\tau\rangle$, is given by

DOI: 10.1021/acs.jpcb.8b10299
J. Phys. Chem. B 2019, 123, 239–246

$$\langle \tau \rangle = \frac{\tau}{\beta}\Gamma\left(\frac{1}{\beta}\right) \quad (26)$$

where $\Gamma(x)$ stands for the gamma function. All three parameters, A, τ, and β are optimized, and the fitting works well, as is demonstrated in Figure 7. The mean relaxation times of $I_{d_0}^{NSE}(Q, t)$ are 0.42 ± 0.07 and 0.421 ± 0.001 ns in the experiment and simulation, respectively, whereas the corresponding values of $I_{combo}(Q,t)$ are 0.87 ± 0.42 and 0.824 ± 0.002 ns, respectively. The agreement between the experiment and the simulation is excellent.

$I_{combo}(Q,t)$ relaxes twice slower than $I_{d_0}^{NSE}(Q, t)$ in both the experiment and MD simulation. Although the slower relaxation of the former cannot be asserted fully confidently from the experiment alone due to the large errors, it is also supported by the MD simulation. There are two possible reasons for the slower relaxation of $I_{combo}(Q,t)$. The first one is the difference in the molecular mobilities in the alkyl and the hydroxyl domains. As $I_{combo}(Q,t)$ probes the dynamics of the cross correlations between the hydrogen atoms in the alkyl and the hydroxyl groups, it is affected by the dynamics of both groups. On the other hand, because $I(Q,t)$ of d_0 is dominated by the contribution of the alkyl group due to the large number of hydrogen atoms, it exclusively probes the dynamics of the alkyl group. The mobility of the hydroxyl group is expected to be lower than that of the alkyl one due to the stronger intermolecular interaction through the hydrogen bonding, which can lead to the slower dynamics of $I_{combo}(Q,t)$. The second one is the retardation of the collective mode by the mesoscopic structure. The presence of the static intermolecular correlation may lead to a slowing down of collective dynamics, as is exemplified by the de Gennes narrowing at the peak of the static structure factor.

The contributions of the alkyl and the hydroxyl groups to the coherent and the incoherent dynamics are calculated separately for the d_{26} sample in Figure 8 to resolve the mechanism of the slow collective relaxation of $I_{combo}(Q,t)$ at the prepeak. Comparing the contributions of the alkyl and the hydroxyl groups, it can be noticed that the relaxation of the latter is slower than that of the former in both the coherent and incoherent parts. The intermolecular hydrogen bonding thus actually retards the dynamics of the hydroxyl group. In addition, the coherent relaxation of the hydroxyl group is slower than the incoherent one. As for the dynamics of the alkyl group, the coherent component has a fast component on the 10 ps time scale, which is not present in the incoherent part. Comparing the relaxation rates after 100 ps, slower dynamics of the coherent part with respect to the incoherent can be discerned in the alkyl group contribution also. This occurrence is ascribed to the mesoscopic structuring originating the prepeak. Both of the two possible mechanisms, the slower dynamics of the hydroxyl group and the intermolecular dynamic correlation, are therefore confirmed in Figure 8, and we consider both of them playing a role in determining the slower relaxation of $I_{combo}(Q,t)$ compared with $I(Q,t)$ of d_0.

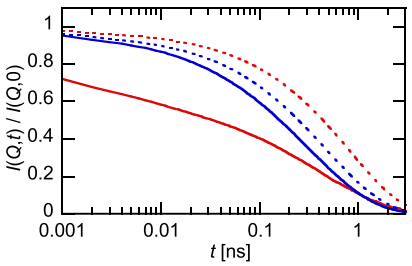

Figure 8. Contributions of the alkyl (solid) and the OH (dotted) groups to the coherent (red) and the incoherent (blue) part of the ISFs to the NSE ISF of d_{26}. These functions are normalized to their respective initial values.

5. SUMMARY

NSE spectroscopy with isotopic substitution was applied to liquid 1-dodecanols to extract the mesoscopic collective dynamics. The collective dynamics at the prepeak was deduced from the linear combination of the ISFs of samples with different degrees of deuteration. MD simulation on the same system was also performed, and the results of the experiment and the simulation agree well.

The collective dynamics at the prepeak is slightly slower than the single particle dynamics determined from the ISF of d_0 sample. The analysis of the MD simulation reveals that there are two mechanisms originating the slower collective dynamics. The first is the hydrogen bonding interaction which slows down the dynamics of the OH group as compared to the alkyl chains, and the other is the mesoscale structuring which affects the intermolecular motions reflected in the collective dynamics. The picture arising, common to 1-alcohols, is the connection between H-bonding, mesoscopic structuring, and slow relaxation modes which originate the bimodality of their viscoelastic relaxation spectra.

AUTHOR INFORMATION

Corresponding Author

*E-mail: yamaguchi.tsuyoshi@material.nagoya-u.ac.jp.

ORCID

Tsuyoshi Yamaguchi: 0000-0003-4590-8592

Notes

The authors declare no competing financial interest.

ACKNOWLEDGMENTS

T.Y. was supported by the Japan Society for the Promotion of Science (JSPS), KAKENHI Grant-in-Aid for Scientific Research (C) (no. 16K05514). Access to the NSE Spectrometer was provided by the Center for High Resolution Neutron Scattering, a partnership between the National Institute of Standards and Technology and the National Science Foundation under agreement no. DMR-1508249. M.N. acknowledges funding support of cooperative agreement 70NANB15H259 from NIST, U.S. Department of Commerce.

ADDITIONAL NOTE

[A]Certain trade names and company products are identified to specify adequately the experimental procedure. In no case does such identification imply our recommendation or endorsement, nor does it imply that the products are necessarily the best for the purpose.

REFERENCES

(1) Bierwirth, S. P.; Bolle, J.; Bauer, S.; Sternemann, C.; Gainaru, C.; Tolan, M.; Böhmer, R. Scaling of suprastructure and dynamics in pure and mixed Debye liquids, In *The Scaling of Relaxation Processes*; Loidl, A., Kremer, F., Eds.; Springer, 2018.

DOI: 10.1021/acs.jpcb.8b10299
J. Phys. Chem. B 2019, 123, 239−246

(2) Tomšič, M.; Bešter-Rogač, M.; Jamnik, A.; Kunz, W.; Touraud, D.; Bergmann, A.; Glatter, O. Nonionic Surfactant Brij 35 in Water and in Various Simple Alcohols: Structural Investigations by Small-Angle X-ray Scattering and Dynamic Light Scattering. *J. Phys. Chem. B* **2004**, *108*, 7021−7032.
(3) Tomšič, M.; Jamnik, A.; Fritz-Popovski, G.; Glatter, O.; Vlček, L. Structural Properties of Pure Simple Alcohols from Ethanol, Propanol, Butanol, Pentanol, to Hexanol: Comparing Monte Carlo Simulations with Experimental SAXS Data. *J. Phys. Chem. B* **2007**, *111*, 1738−1751.
(4) Kaatze, U.; Behrends, R. High-Frequency Shear Viscosity of Low-Viscosity Liquids. *Int. J. Thermophys.* **2014**, *35*, 2088−2106.
(5) Gainaru, C.; Figuli, R.; Hecksher, T.; Jakobsen, B.; Dyre, J. C.; Wilhelm, M.; Böhmer, R. Shear-Modulus Investigations of Monohydroxy Alcohols: Evidence for a Short-Chain-Polymer Rheological Response. *Phys. Rev. Lett.* **2014**, *112*, 098301.
(6) Gainaru, C.; Wikarek, M.; Pawlus, S.; Paluch, M.; Figuli, R.; Wilhelm, M.; Hecksher, T.; Jakobsen, B.; Dyre, J. C.; Böhmer, R. Oscillatory shear and high-pressure dielectric study of 5-methyl-3-heptanol. *Colloid Polym. Sci.* **2014**, *292*, 1913−1921.
(7) Hecksher, T. Communication: Linking the dielectric Debye process in mono-alcohols to density fluctuations. *J. Chem. Phys.* **2016**, *144*, 161103.
(8) Arrese-Igor, S.; Alegría, A.; Colmenero, J. Multimodal character of shear viscosity response in hydrogen bonded liquids. *Phys. Chem. Chem. Phys.* **2018**, *20*, 27758.
(9) Yamaguchi, T. Viscoelastic relaxations of high alcohols and alkanes: Effects of heterogeneous structure and translation-orientation coupling. *J. Chem. Phys.* **2017**, *146*, 094511.
(10) Yamaguchi, T.; Saito, M.; Yoshida, K.; Yamaguchi, T.; Yoda, Y.; Seto, M. Structural Relaxation and Viscoelasticity of a Higher Alcohol with Mesoscopic Structure. *J. Phys. Chem. Lett.* **2018**, *9*, 298−301.
(11) Witten, T.; Pincus, P. *Structured Fluids: Polymers, Colloids, Surfactants*; Oxford University Press: Oxford, U.K., 2004.
(12) Yamaguchi, T.; Mikawa, K.-i.; Koda, S.; Fujii, K.; Endo, H.; Shibayama, M.; Hamano, H.; Umebayashi, Y. Relationship between mesoscale dynamics and shear relaxation of ionic liquids with long alkyl chain. *J. Chem. Phys.* **2012**, *137*, 104511.
(13) Yamaguchi, T.; Yonezawa, T.; Koda, S. Study on the temperature-dependent coupling among viscosity, conductivity and structural relaxation of ionic liquids. *Phys. Chem. Chem. Phys.* **2015**, *17*, 19126−19133.
(14) Yamaguchi, T.; Yonezawa, T.; Yoshida, K.; Yamaguchi, T.; Nagao, M.; Faraone, A.; Seki, S. Relationship between Structural Relaxation, Shear Viscosity, and Ionic Conduction of LiPF6/Propylene Carbonate Solutions. *J. Phys. Chem. B* **2015**, *119*, 15675−15682.
(15) Yamaguchi, T. Experimental study on the relationship between the frequency-dependent shear viscosity and the intermediate scattering function of representative viscous liquids. *J. Chem. Phys.* **2016**, *145*, 194505.
(16) Yamaguchi, T.; Yoshida, K.; Yamaguchi, T.; Nagao, M.; Faraone, A.; Seki, S. Decoupling Between the Temperature-Dependent Structural Relaxation and Shear Viscosity of Concentrated Lithium Electrolyte. *J. Phys. Chem. B* **2017**, *121*, 8767−8773.
(17) Yamaguchi, T.; Faraone, A. Analysis of shear viscosity and viscoelastic relaxation of liquid methanol based on molecular dynamics simulation and mode-coupling theory. *J. Chem. Phys.* **2017**, *146*, 244506.
(18) Sillrén, P.; Matic, A.; Karlsson, M.; Koza, M.; Maccarini, M.; Fouquet, P.; Götz, M.; Bauer, T.; Gulich, R.; Lunkenheimer, P.; Loidl, A.; Mattsson, J.; Gainaru, C.; Vynokur, E.; Schildmann, S.; Bauer, S.; Böhmer, R. Liquid 1-propanol studied by neutron scattering, near-infrared, and dielectric spectroscopy. *J. Chem. Phys.* **2014**, *140*, 124501.
(19) Finney, J. L.; Soper, A. K. Solvent structure and perturbations in solutions of chemical and biological importance. *Chem. Soc. Rev.* **1994**, *23*, 1−10.
(20) Faraone, A.; Hong, K.; Kneller, L. R.; Ohl, M.; Copley, J. R. D. Coherent dynamics of meta-toluidine investigated by quasielastic neutron scattering. *J. Chem. Phys.* **2012**, *136*, 104502.
(21) Faraone, A.; Wagle, D. V.; Baker, G. A.; Novak, E. C.; Ohl, M.; Reuter, D.; Lunkenheimer, P.; Loidl, A.; Mamontov, E. Glycerol Hydrogen-Bonding Network Dominates Structure and Collective Dynamics in a Deep Eutectic Solvent. *J. Phys. Chem. B* **2018**, *122*, 1261−1267.
(22) Bertrand, C. E.; Self, J. L.; Copley, J. R. D.; Faraone, A. Nanoscopic length scale dependence of hydrogen bonded molecular associates' dynamics in methanol. *J. Chem. Phys.* **2017**, *146*, 194501.
(23) Bée, M. *Quasielastic Neutron Scattering: Principles and Applications in Solid State Chemistry, Biology and Materials Science*; A. Hilger: Bristol; Philadelphia, 1988.
(24) Monkenbush, M.; Richter, D. Neutron Spin Echo Spectroscopy. In *Neutrons in Soft Matter*; Imae, T., Kanaya, T., Furusaka, M., Torikai, N., Eds.; John Wiley & Sons, 2011.
(25) Gaspar, A. M.; Busch, S.; Appavou, M.-S.; Haeussler, W.; Georgii, R.; Su, Y.; Doster, W. Using polarization analysis to separate the coherent and incoherent scattering from protein samples. *Biochim. Biophys. Acta* **2010**, *1804*, 76−82.
(26) Abraham, M. J.; Murtola, T.; Schulz, R.; Páll, S.; Smith, J. C.; Hess, B.; Lindahl, E. GROMACS: High performance molecular simulations through multi-level parallelism from laptops to supercomputers. *SoftwareX* **2015**, *1*−*2*, 19−25.
(27) Riddick, J. A.; Bunger, W. B.; Sakano, T. K. *Organic Solvents*, 4th ed.; John Wiley & Sons: New York, 1986.
(28) Martin, M. G.; Siepmann, J. I. Transferable Potentials for Phase Equilibria. 1. United-Atom Description ofn-Alkanes. *J. Phys. Chem. B* **1998**, *102*, 2569−2577.
(29) Chen, B.; Potoff, J. J.; Siepmann, J. I. Monte Carlo Calculations for Alcohols and Their Mixtures with Alkanes. Transferable Potentials for Phase Equilibria. 5. United-Atom Description of Primary, Secondary, and Tertiary Alcohols. *J. Phys. Chem. B* **2001**, *105*, 3093−3104.

DOI: 10.1021/acs.jpcb.8b10299
J. Phys. Chem. B 2019, 123, 239−246